Gap-junction coupling and ATP-sensitive potassium channels in human β-cell clusters: Effects on emergent dynamics

A. Loppini,[1] M. G. Pedersen,[2] M. Braun,[3,*] and S. Filippi[1]

[1]*Nonlinear Physics and Mathematical Modeling Laboratory, Campus Bio-Medico University of Rome, I-00128 Rome, Italy*

[2]*Department of Information Engineering, University of Padua, I-35131 Padua, Italy*

[3]*Alberta Diabetes Institute, Department of Pharmacology, University of Alberta, Edmonton, T6G 2H7 Alberta, Canada*

(Received 9 January 2017; published 6 September 2017)

The importance of gap-junction coupling between β cells in pancreatic islets is well established in mouse. Such ultrastructural connections synchronize cellular activity, confine biological heterogeneity, and enhance insulin pulsatility. Dysfunction of coupling has been associated with diabetes and altered β-cell function. However, the role of gap junctions between human β cells is still largely unexplored. By using patch-clamp recordings of β cells from human donors, we previously estimated electrical properties of these channels by mathematical modeling of pairs of human β cells. In this work we revise our estimate by modeling triplet configurations and larger heterogeneous clusters. We find that a coupling conductance in the range 0.005–0.020 nS/pF can reproduce experiments in almost all the simulated arrangements. We finally explore the consequence of gap-junction coupling of this magnitude between β cells with mutant variants of the ATP-sensitive potassium channels involved in some metabolic disorders and diabetic conditions, translating studies performed on rodents to the human case. Our results are finally discussed from the perspective of therapeutic strategies. In summary, modeling of more realistic clusters with more than two β cells slightly lowers our previous estimate of gap-junction conductance and gives rise to patterns that more closely resemble experimental traces.

DOI: 10.1103/PhysRevE.96.032403

I. INTRODUCTION

β cells in the endocrine pancreas release insulin in response to high glucose levels in the blood. Animal studies have shown that β cells coordinate their activity through gap-junction coupling, leading to a robust and synchronized response to glucose stimulation that enhances insulin pulsatility [1–4]. Loss of coupling was shown to have detrimental effects on β-cells functionality, causing impaired hormone secretion [5–7]. Despite gap-junction forming proteins (mostly Connexin-36) being expressed also in human islets [8], the role of such coupling on human β cells' electrical activity and insulin secretion is still unexplored. In a previous study [9], we estimated the coupling conductance between human β cells by using a comprehensive electrophysiological model [10,11] and patch-clamp membrane voltage recordings from small human β-cell clusters. Simulations performed on cell doublets showed that gap-junction coupling should be in the range 0.010–0.020 nS/pF to reproduce experimental recordings, an estimate in agreement with reported values of gap-junction conductance in coupled mouse β cells [12–14]. A value of coupling conductance equal to the lower limit of the estimated range was large enough to significantly affect electrical behavior, promoting synchronized spiking activity and enhancement of fast bursting oscillations, and could cause fragmentation or synchronization of glycolysis-driven bursting [9].

We investigate here the sensitivity of our estimate of gap-junction conductance to changes in β-cell cluster size. Specifically, our results show that a coupling conductance within the range 0.005–0.020 nS/pF can reproduce patch-clamp data when considering assemblies of three cells. In this case, heterogeneity in cells' spiking activity induce irregular membrane potential oscillations that are observed in experimental recordings, and which were not reproduced by cell doublets [9]. Furthermore, we show that this revised range of coupling strengths can fit experimental observations also in the case of larger cubic clusters. Finally, we investigate the role of electrical coupling in pathological β-cells clusters by mimicking assemblies of normal cells intermingled with cells expressing mutant KATP channels. Such mutant variants of ATP-sensitive potassium channels, which show inactivity or overactivity with respect to normal functioning channels, are implicated in metabolic disorders and diabetic conditions [15–18]. In this regard, modulation of coupling in mouse was shown to recover β-cell activity partially restoring insulin secretion [19–21]. Our results show that, in mosaic assemblies of normal and pathological human β cells, electrical coupling induces overinhibition or overexcitation of the cluster and significantly alters the global dose-response curve. Lowering of gap-junction conductance may prevent detrimental entrainment of the normally functioning cells and recover their functionality.

The paper is organized as follows. Section II gives a description of both the experimental signals and mathematical model, discussing also numerical implementation of the algorithm. Obtained results are presented in Sec. III. Section IV is devoted to conclusions and study implications. Limits of the model and future perspectives are also outlined.

II. MATERIALS AND METHODS

We previously reported small-amplitude oscillations in the membrane potential of a patched human β cell within a tiny cluster of cells stimulated by 6 mM glucose (Fig. 1 here, Fig. 2 in Ref. [9]). In control conditions, such patterns consist of oscillations of $\simeq$10 mV from a baseline of about -50 mV, occasionally triggering action potential firing. Exposure to

[*]Deceased.

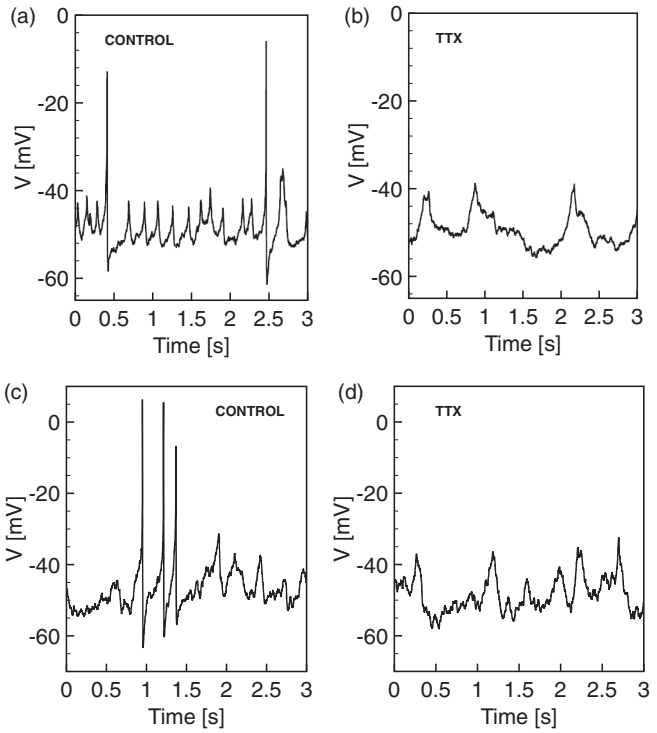

FIG. 1. Experimental patch-clamp recordings of two β cells within small clusters. (a) Cell 1 in control condition. (b) Cell 1 during TTX exposure. (c) Cell 2 in control condition. (d) Cell 2 during TTX exposure. Experimental details can be found in Ref. [9].

the sodium channel blocker TTX suppresses action potential firing and reduces the frequency of the small-amplitude oscillations without changing their amplitude. Considering heterogeneity in glucose responsiveness, we hypothesized that such oscillations are due to coupling currents coming from neighboring active cells, perturbing the silent state of the patched cell.

With the aim to reproduce recorded signals, a Hodgkin-Huxley-type model was used here to simulate human β-cell electrophysiology [9–11]. Such a formulation takes into account all the significant ion currents that were experimentally characterized in human electrophysiological studies [22–26]. As in previous works [9,27–30], a diffusive term was added to the equation for membrane voltage to model gap-junction induced currents,

$$\frac{dV_i}{dt} = -I_{\mathrm{ion},i} - g_c \sum_{j\in\Omega}(V_i - V_j), \qquad (1)$$

where $I_{\mathrm{ion},i}$ is the sum of the ionic currents through the membrane, g_c is the coupling conductance, and Ω is the neighborhood of the cell defined by the considered cell-cluster topology. Specifically, we modeled configurations with three cells, i.e., triangles and chains, and three-dimensional $n\times n\times n$ clusters of cells in which central cells are coupled to six neighbors. This choice is in line with neighborhood size measured in mouse islets (about seven cells), and with reduced β-cell fraction in human islet [14,31–33], although other modeling studies considered hexagonal packaging of cells which allow neighborhoods of 12 cells in size [34,35]. A complete list of model equations and parameters can be found in Appendix A.

Biological heterogeneity was introduced by varying the g_{KATP}, $g_{\mathrm{Ca}T}$, g_{leak}, and g_{Na} ion conductance parameters, keeping the other parameters fixed at their default values [9], which permitted reproducing different types of β cells, showing either fast spiking, slow spiking, or no electrical activity in response to glucose. In the case of heterogeneous clusters, we further normally distributed the g_{KATP} or $g_{\mathrm{K}v}$ parameters with different means and standard deviations. The three-cell configurations were resolved with the XPPAUT software [36], suited for analysis of dynamical systems, by using a CVODE algorithm for the integration of the ordinary differential equations (ODEs). Bifurcation points and curves were numerically computed and classified with AUTO (within XPPAUT). In the case of larger cell clusters, the model was implemented in a C++ algorithm and the ODE system was resolved with a fourth-order Runge-Kutta numerical scheme by adopting a fixed time step $dt = 0.01$ ms. This choice ensured both reasonable computing time and good accuracy of results. The latter was checked by reducing the time step fivefold ($dt = 0.002$ ms) in control simulations, which did not improve accuracy.

III. RESULTS

We previously estimated gap-junction conductance between human β cells by hypothesizing that the small amplitude oscillations recorded in patch-clamp experiments represent perturbations of a silent patched cell evoked by gap-junction currents coming from neighboring active cells (see Sec. II). Simulations of cell doublets, formed by a spiking and a silent cell, showed that a gap-junction conductance in the range 0.010–0.020 nS/pF is required to sustain small oscillations in the silent cell with amplitude similar to experiment recordings [9]. However, since the exact number of cells contained in the experimental clusters is unknown, it is possible that the coupling parameter was overestimated. Here we investigate the robustness of our estimate when more than two cells are coupled, by searching for suitable values of the coupling strength that correctly reproduce the emergent oscillations. Implications of this estimate on the emergent behavior of pathological aggregates of cells are finally analyzed.

A. Three-cell configurations

In configurations with three cells, the silent patched cell is coupled to two neighboring cells. Because of cell heterogeneity, different scenarios have to be considered. For instance, the silent patched cell can be coupled to a pair of active β cells, showing fast spiking activity in response to glucose. Alternatively, the patched cell could be coupled to a fast spiking cell and to a nonresponsive cell. Finally, triplets could be formed by two spiking cells characterized by different spike frequencies, i.e., fast and slow spikers, driving junctional inputs into the silent patched cell. To further enrich the picture, the triplets may show either a triangular or a chain topology, where the two neighboring cells are directly coupled or not, respectively. Note that chain configurations with the silent patched cell located in the

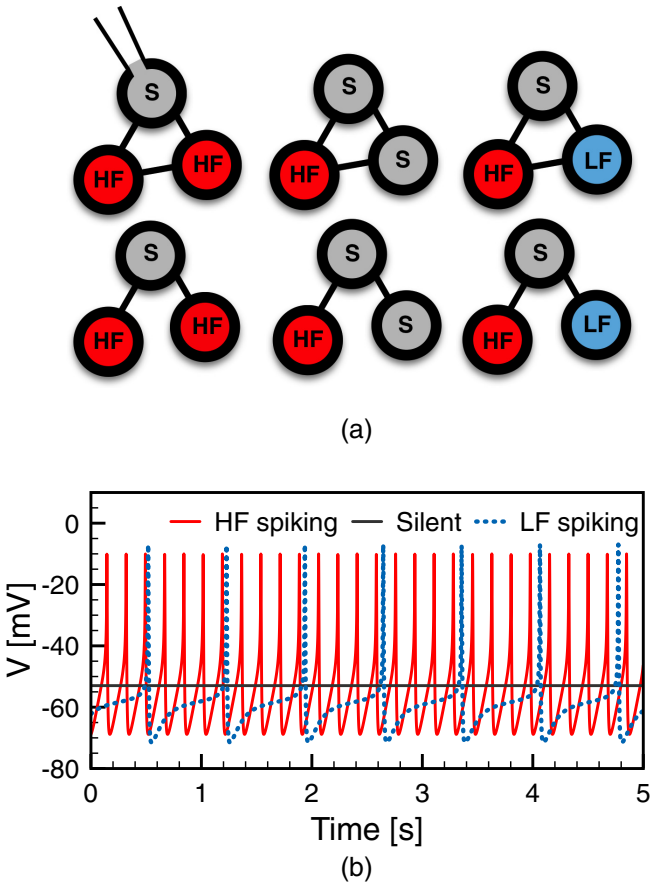

FIG. 2. (a) Triangular and chain topologies of β-cell triplets. HF, high-frequency spiking cell; S, silent cell; LF, low-frequency spiking cell. The top vertex is the patched silent β cell. Left column: HF-S-HF configuration. Central column: HF-S-S configuration. Right column: HF-S-LF configuration. (b) Model simulations showing membrane potential of isolated HF, LF, and S cells.

outer positions were not considered, since we are mainly interested in testing the estimate of coupling strength in the case of gap-junction currents coming from more than one neighboring cell. Figure 2(a) represents the described scenarios. On this basis, we modeled the mentioned β-cell triplets investigating evoked oscillations in the silent patched cell. Specifically, silent (S) and high-frequency spiking (HF) cells were modeled by properly setting the conductance value of the ATP-sensitive potassium channel, while low-frequency (LF) spiking dynamics was obtained by fine-tuning of the leakage, calcium, sodium, and KATP conductance with respect to the original value of the parameters (see Table I). Computed membrane potential traces of isolated S, HF, and LF cells are shown in Fig. 2(b).

When considering two identical fast spiking cells coupled to a silent one [HF-S-HF, left column in Fig. 2(a)], the triangular and chain topologies are equivalent because of the identical dynamics of the two HF cells and symmetric coupling. The amplitude of membrane potential oscillations evoked in the silent cell was computed in the triangle configuration at different values of the coupling strength (g_c) and KATP conductance of the HF cells ($g_{\mathrm{KATP_{HF}}}$), in order to investigate sensitivity

TABLE I. Model parameters adopted to reproduce silent (S), low-frequency (LF), and high-frequency (HF) spiking activity. All values are reported in nS/pF.

	S	LF	HF
g_{KATP}	0.020	0.025	0.005/0.010
$g_{\mathrm{Ca}T}$	0.05	0.50	0.05
g_{Na}	0.4	0	0.4
g_{leak}	0.0150	0.0075	0.0150

to the activation level of the fast spikers. The two-parameter bifurcation diagram in Fig. 3(a) shows that by lowering the $g_{\mathrm{KATP_{HF}}}$ conductance value, i.e., by increasing the fast spiker activation level, the system undergoes a Hopf bifurcation and small-amplitude periodic oscillations arise in the silent patched cell. Results show that, in control conditions with $g_c \geqslant 0.010$ nS/pF and $g_{\mathrm{KATP_{HF}}}$ lower than a transition threshold (Hopf bifurcation curves in Fig. 3) evoked oscillations are too large, while an amplitude of $\simeq$10 mV is obtained for g_c in the range 0.005–0.010 nS/pF [see Figs. 3(a) and 3(d)]. When the same triplet is exposed to TTX, higher activation levels of the HF cells are required to ensure an oscillatory regime. However, an amplitude of $\simeq$10 mV can still be observed for g_c in the range 0.005–0.010 nS/pF, as for the control case [Figs. 3(b) and 3(e)]. These considerations are almost independent of $g_{\mathrm{KATP_{HF}}}$, in both control and TTX conditions.

In the case of a patched cell coupled to a HF spiker and a silent β cell [HF-S-S, central column in Fig. 2(a)], the evoked oscillations change significantly compared to the HF-S-HF configuration. In control conditions, when the HF cell is sufficiently activated to overcome the silencing effect of the other cells, a chain topology induces oscillations comparable to experiments for g_c in the range 0.015–0.020 nS/pF [Figs. 3(c) and 3(f)]. However, when TTX exposure is simulated (not shown), oscillations with appropriate amplitude are recovered only for higher values of coupling (>0.020 nS/pF) and for strongly activated HF cells ($g_{\mathrm{KATP_{HF}}} \simeq 0.002$ nS/pF). Similar results were obtained for the HF-S-S configuration in a triangular topology, where an additional link between the outer S and HF cells enhances the silencing effect. In this case, strong activation of the HF cell and $g_c \simeq 0.020$ nS/pF reproduced experimental oscillations in control condition. However, higher values of coupling (>0.020 nS/pF) inhibited HF cell spiking in both control and TTX conditions. In addition, during TTX exposure the HF-S-S triangle was never able to generate oscillations comparable to the patch-clamp recordings (not shown).

Nontrivial emerging behavior is obtained when the patched S cell is coupled to a fast spiker and a slow spiker cell [HF-S-LF, right column in Fig. 2(a)]. A chain topology gives rise to irregular oscillations, which are not possible to track in a two-parameter bifurcation diagram, as for the previous cases. Maxima and minima of the irregular oscillations were thus computed at selected activation levels of the HF cell by varying g_c (Fig. 4). Results show that significant features of the experimental signals are reproduced with different sets of the parameters. When the HF cell is mildly activated ($g_{\mathrm{KATP_{HF}}} =$ 0.010 nS/pF), a coupling conductance equal to 0.010 nS/pF

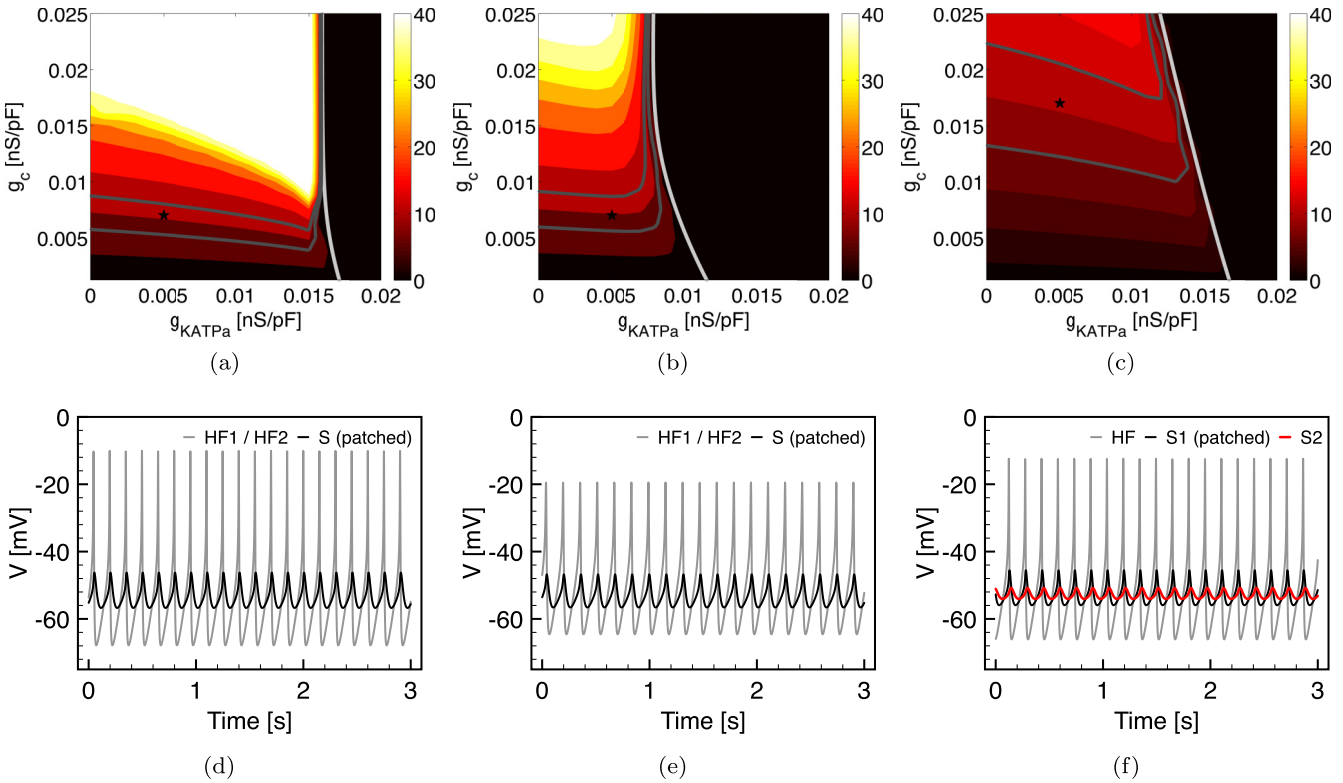

FIG. 3. Two-parameter bifurcation diagrams computed on selected triplets [(a)–(c)], showing membrane potential oscillations evoked in the patched cell. Simulated membrane potential signals are also shown for selected points [(d)–(f)] [black asterisks in (a), (b), and (c)]. Diagrams were obtained by varying the KATP conductance of the active HF cell (g_{KATP_a}) and the coupling conductance g_c. (a) HF-S-HF triangle configuration in control condition. (b) HF-S-HF triangle configuration during TTX exposure. (c) HF-S-S chain configuration in control condition. The thick light gray curve is the boundary between oscillatory solutions and stable fixed points, i.e., the Hopf bifurcations curve. Thick dark-gray curves highlight oscillations in the range 8–12 mV. Color bar denotes the oscillation amplitude in millivolts. (d) Computed membrane potentials in a HF-S-HF triangle in control condition with $g_{\mathrm{KATP}_a} = 0.005$ nS/pF and $g_c = 0.007$ nS/pF. (e) Computed membrane potentials in a HF-S-HF triangle during TTX exposure with $g_{\mathrm{KATP}_a} = 0.005$ nS/pF and $g_c = 0.007$ nS/pF. (f) Computed membrane potentials in a HF-S-S chain in control condition with $g_{\mathrm{KATP}_a} = 0.005$ nS/pF and $g_c = 0.017$ nS/pF.

is able to induce irregular, possibly chaotic, oscillations of about 10 mV in amplitude [Fig. 4(a)]. Interestingly, when TTX exposure is simulated, evoked oscillations regularize, but with unchanged amplitude. Moreover, such regularization seems to reduce the frequency of the signal [Figs. 4(b) and 4(c)]. When the HF cell is strongly activated ($g_{\mathrm{KATP}_{\mathrm{HF}}} = 0.005$ nS/pF), different interesting patterns are observed [Figs. 4(d) and 4(e)]. At $g_c \simeq 0.01$ nS/pF, a period-3 oscillation with amplitudes comparable to experimentally observed excursions is obtained. In this case, TTX exposure does not regularize membrane potential dynamics in the patched cell and oscillations become chaoslike, despite the maximum amplitude being only minimally affected. At $g_c \simeq 0.018$ nS/pF the patched S cell shows chaoslike oscillations with small peaks ($\simeq$10 mV) intermingled with large oscillations resembling spikes [Fig. 4(f)]. This pattern nicely resembles the experimentally recorded signals, which present occasional spikes together with small perturbations. In this case, exposing the triplet to TTX regularizes oscillation amplitude, suppresses occasional spikes, and slightly lowers the oscillation frequency, although less markedly compared to the case with lower coupling strength and milder activation of the HF cell.

Finally, we tested a triangular topology for the HF-S-LF triplet. In this case no irregular oscillations were observed due to synchronization of the HF and LF cells, promoted by the additional link. In comparison with the chain topology, similar results in terms of evoked oscillation amplitude were obtained.

In summary, simulations of cell triplets suggest that a coupling conductance in the range 0.005–0.020 nS/pF can accurately reproduce experimental patch-clamp data in most of the hypothesized configurations. In addition, some of these arrangements can explain complex features of the emergent activity that were not reproduced by smaller assemblies of cells.

B. Small clusters

Analyses on β-cell triplets show that when a silent cell is coupled to two spiking cells, a gap-junction conductance lower than 0.010 nS/pF is required to reproduce 10 mV evoked oscillations. However, when larger neighborhoods are considered, nonresponsive adjacent cells could, in principle, balance the additional stimulatory coupling current due to an enhanced silencing effect, possibly shifting the required g_c to higher values. In order to investigate evoked oscillations in the case of a higher number of neighboring β cells, we modeled small cubic clusters of 8 and 27 cells [Figs. 5(a) and 5(d)] formed by heterogeneous populations of S, LF, and

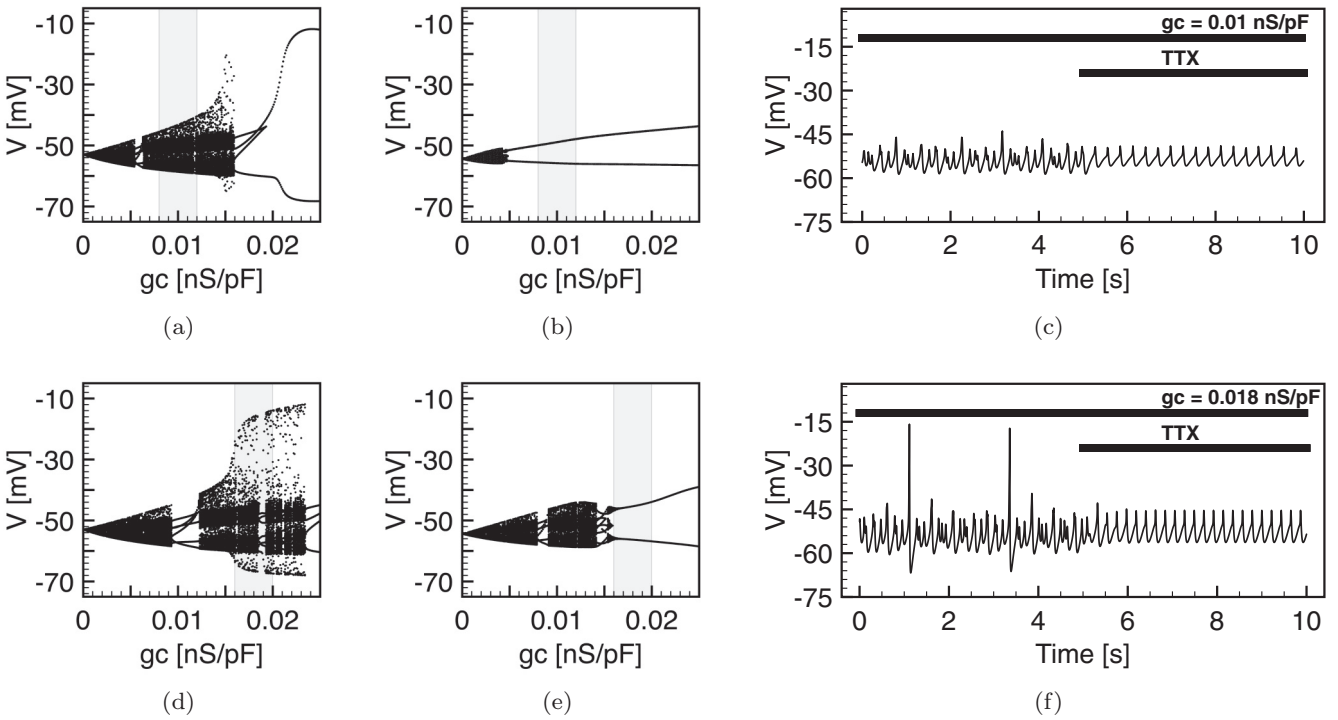

FIG. 4. Maxima and minima of membrane potential oscillations evoked in the silent patched cell in a HF-S-LF triplet versus the coupling conductance g_c [(a),(b),(d),(e)]. Computed membrane is shown at selected values of coupling strength and HF spiker activation level [(c),(f)]. (a) Control condition and mild activation ($g_{KATP} = 0.01$ nS/pF) of the fast spiking cell. (b) TTX exposure ($g_{Na} = 0$ nS/pF) and mild activation ($g_{KATP} = 0.01$ nS/pF) of the fast spiking cell. (c) Computed membrane potential of the patched cell with $g_c = 0.01$ nS/pF; activation level of the fast spiker as in (a) and (b); TTX exposure is modeled by setting $g_{Na} = 0$ nS/pF at $t = 5$ s. (d) Control condition and strong activation ($g_{KATP} = 0.005$ nS/pF) of the fast spiking cell. (e) TTX exposure ($g_{Na} = 0$ nS/pF) and strong activation ($g_{KATP} = 0.005$ nS/pF) of the fast spiking cell. (f) Computed membrane potential of the patched cell with $g_c = 0.018$ nS/pF; activation level of the fast spiker as in (d) and (e); TTX exposure is modeled by setting $g_{Na} = 0$ nS/pF at $t = 5$ s.

HF cells. Populations heterogeneity was modeled by normally distributing the KATP conductance with a mean value equal to the original parameter (see Fig. 2) and a standard deviation equal to 10% for S and HF cell types, and equal to 1% for the LF type to ensure a low-frequency spiking behavior. Interestingly, when cells are coupled with $g_c = 0.010$ nS/pF evoked oscillation with an amplitude of $\simeq$10 mV can be observed both in control condition and during TTX exposure, both in the 8 and 27 cells clusters [Figs. 5(b) and 5(e)]. Such emergent behavior can arise also in HF cells due to the silencing effect induced by neighboring unresponsive cells, and not only in S cells trapped in small-amplitude oscillatory regimes [Fig. 5(e)]. This finding supports the idea of a balancing effect of polarizing and depolarizing gap-junction currents, which causes oscillations comparable to experiments for $g_c = 0.010$ nS/pF. When the coupling is reduced to $g_c = 0.005$ nS/pF a complex activity arises, in line with the HF-S-LF triplet configuration discussed above. In particular, irregular oscillations in which large spikes are intermingled with small oscillations can be observed in the 27 cells cluster. When the same cluster is exposed to TTX, large oscillations are suppressed. In the case of eight cells, irregular oscillations of $\simeq$5 mV are observed in control conditions. These oscillations are not suppressed by TTX exposure, which induces a clear reduction in frequency. This reduction is more pronounced compared to the triplet case and more consistent with patch-clamp recordings.

Overall, the analysis of small clusters confirmed that the gap-junction conductance range, previously estimated from doublets, must be corrected to also include lower values (0.005 nS/pF), thus we consider 0.010 nS/pF as an average strength more than a lower bound.

C. Mutant KATP

The previous analyses were mainly focused on finding the gap-junction conductance value that correctly reproduces features in the experimental traces. Quantifying gap-junction strength is a key point not only to understand β-cell dynamics in the physiological scenario, but it is also useful to investigate cellular response in a pathological regime. For instance, several studies have shown that mutant variants of KATP channels have significant effects on emergent dynamics of mouse β-cells clusters, with severe implications for insulin secretion [18,19]. Indeed, such mutant ion channels, showing hyperactivity (gain-of-function) or inactivity (loss-of-function) with respect to normal functioning channels, are involved in some forms of diabetes or hyperinsulinemia [15–17]. Modulation of coupling conductance was shown in mouse to partially recover normal β-cell function in heterogeneous

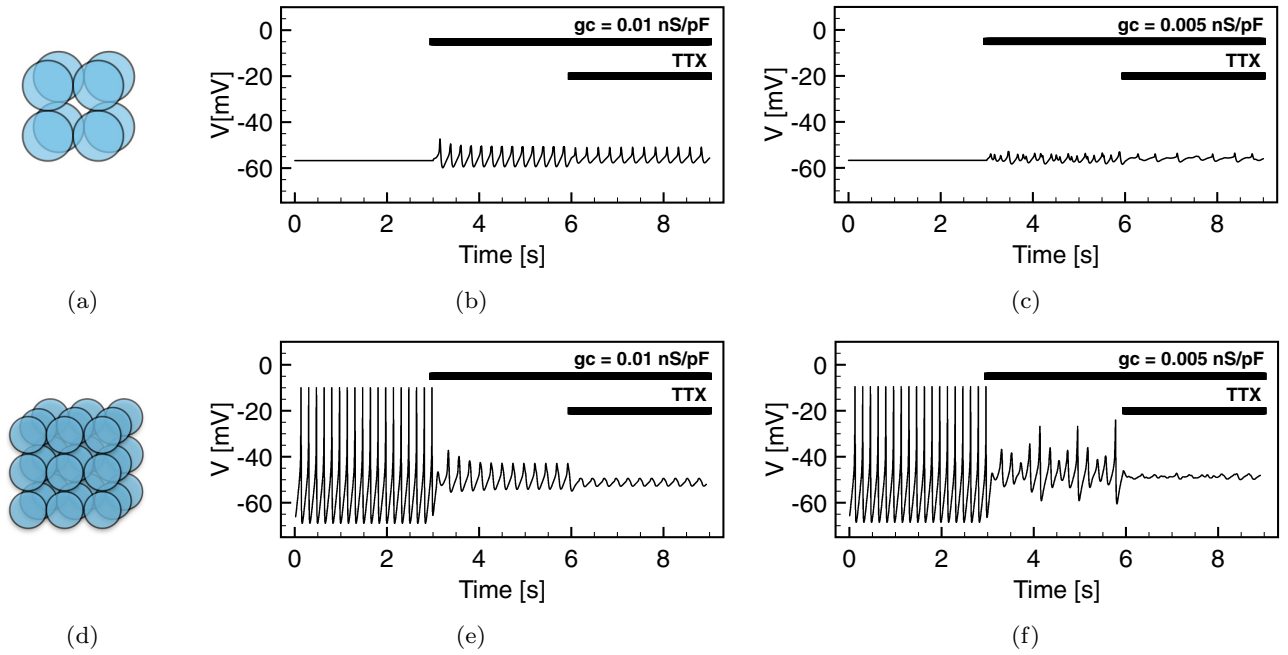

FIG. 5. Membrane potential of selected β cells within 2×2×2 (a) and 3×3×3 (d) coupled clusters. (b) Membrane potential of a silent cell located on the vertex of the cluster shown in (a), $g_c = 0.01$ nS/pF. (c) Same simulation as in (b), but with $g_c = 0.005$ nS/pF. (e) Membrane potential of a fast spiking cell located at the center of the cluster shown in (d), $g_c = 0.01$ nS/pF. (f) Same simulation as in (e), but with $g_c = 0.005$ nS/pF. At $t = 3$ s the electrical coupling is turned on, and at $t = 6$ s the cluster is exposed to TTX by setting $g_{\mathrm{Na}} = 0$ nS/pF.

populations composed of normal and KATP-mutant cells, both considering gain-of-function and loss-of-function mutations [20,29,37]. In particular, experiments on engineered mouse islets, formed by a mosaic arrangement of normal and mutant cells, were performed to enlighten the role of coupling in these pathological regimes [37]. In light of these experiments, we analyzed a similar scenario where normal responding human β cells are mixed with hyperactive or inactive cells, investigating the effect of electrical coupling on the emergent activity of the cluster. Specifically, we modeled 27-cells cubic clusters with fixed percentages of cells showing mutant ATP-sensitive potassium channels: (1) 30% mutant and 70% normal HF cells and (2) 70% mutant and 30% normal HF cells. To test cluster functionality, we obtained a dose-response curve by computing at different glucose concentrations the average value of cytosolic calcium over the whole cluster, i.e., $\langle X_{\mathrm{Ca}_c} \rangle = \frac{1}{N_{\mathrm{cell}}} \sum_{i=1}^{N_{\mathrm{cell}}} \overline{X^i_{\mathrm{Ca}_c}}$, where $\overline{X^i_{\mathrm{Ca}_c}}$ is the mean intracellular calcium concentration for the ith cell $\overline{X^i_{\mathrm{Ca}_c}} = \frac{1}{T} \int_0^T X^i_{\mathrm{Ca}_c}(t)dt$ and $T = 3$ s is the simulation time. Both gain-of-function and loss-of-function mutations were modeled by keeping the g_{KATP} parameter of pathological cells fixed at subthreshold (0.035 nS/pF) or stimulatory values (0.005 nS/pF), while glucose stimulation was modeled by varying the g_{KATP} conductance of normal HF cells. With this approach pathological cells do not respond to glucose and show a hyperpolarized or spiking state depending on the mutation type. In addition, heterogeneity in cell populations was introduced by normally distributing the delayed rectifying potassium conductance g_{Kv}, with a mean value equal to the original parameter (1 nS/pF) and a standard deviation equal to 10%.

Cells expressing KATP gain-of-function mutations are not able to depolarize due to overactivity of KATP channels. In this case, results show that 30% of cells expressing mutant channels are enough to lower mean calcium value across the cluster in a stimulating range of glucose [Fig. 6(a)]. This detrimental effect is more pronounced when the percentage of pathological cells increases up to 70% [Fig. 6(b)]. In particular, setting g_c at the estimated physiological mean value $\simeq$0.010 nS/pF, silent cells force the normal spikers into a polarized state, preventing calcium increase. However, when the coupling conductance is lowered by a factor $\simeq$20 (0.0005 nS/pF), the β-cells' response is partially recovered at glucose concentrations slightly above the stimulation threshold. In addition, the glucose range in which calcium oscillations are partly recovered is larger in the case of 70% mutant cells.

When loss-of-function mutations are considered, pathological cells are in a depolarized state because of KATP channels inactivity. Such hyperactive cells induce a basal increase of the average intracellular calcium concentration. Interestingly, in the case of 30% mutant cells a coupling conductance equal to 0.020 nS/pF is able to mitigate this phenomenon thanks to the silencing effect of normally responding cells, which keeps mutant cells polarized even at glucose concentrations far below the activation threshold. However, at increasing glucose levels, coupling has an opposite effect, driving normal responding cells into a depolarized state prematurely [Fig. 6(c)]. Within the same range of glucose stimulation, a lowering in the coupling conductance by a factor >2 results in a dose-response profile closer to the normal one, where all cells respond physiologically to glucose when coupled with $g_c = 0.010$ nS/pF. In the case of a high percentage of mutant

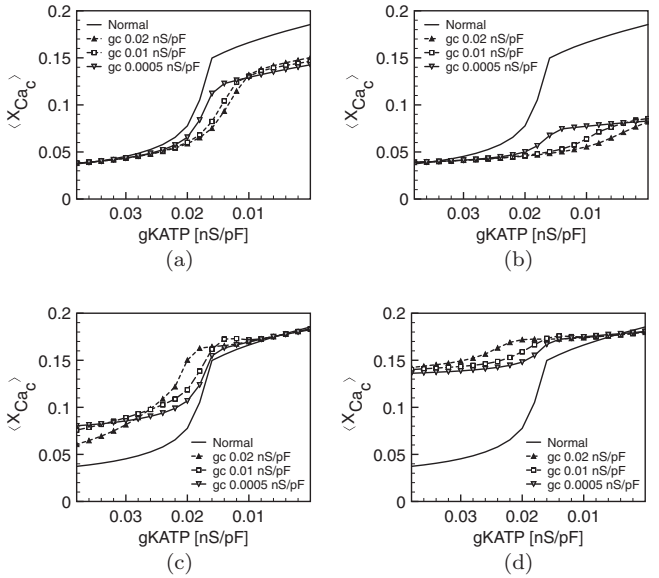

FIG. 6. Dose-response curves showing average value of intracellular calcium over the clusters computed on 3 s of simulated activity. (a) 30% gain-of-function KATP mutant cells (inactive) and 70% normal spiking cells. (b) 70% gain-of-function KATP mutant cells and 30% normal spiking cells. (c) 30% loss-of-function KATP mutant cells (hyperactive) and 70% normal spiking cells. (d) 70% loss-of-function KATP mutant cells and 30% normal spiking cells. "Normal" case denotes a cluster formed by 100% normal spiking cells coupled with $g_c = 0.01$ nS/pF. Average calcium value $\langle Ca \rangle$ is expressed in μM. Note that the g_{KATP} scale on the x axes has been inverted so that it corresponds to increasing glucose levels.

overactive cells (70%), the effect of coupling is detrimental [Fig. 6(d)]. Specifically, normal cells at subthreshold glucose are depolarized by gap-junction induced perturbations coming from mutant cells. Low coupling strengths ($\simeq$0.0005 nS/pF) minimally restore a normal dose-response profile, by inhibition of depolarization induced by overactive cells.

IV. DISCUSSION

Gap-junction coupling is known to be a key aspect of β-cells function in mouse [7,38–41] and it has been shown that down-regulation of proteins forming junctional channels is associated with impaired insulin secretion and diabetic states [5,42–46]. Considering this, several studies have focused on characterizing the distribution of gap-junction connections between β cells in mouse islets and on measuring electrical properties via patch-clamp experiments, or via dye diffusion and imaging techniques [12–14,47,48]. Recent studies have shown that Connexin proteins forming gap junctions are expressed also in human islets [8], despite the differences in cellular composition and architecture with respect to mouse islets. In fact, histological investigations pointed out that the β-cell fraction is lower and more variable in humans, and that β cells are not compactly located in the islet core but seem to be scattered randomly throughout the islet, or at most forming small clusters intermingled with other types of cells [31–33]. In addition, mouse and human β cells also present electrophysiological differences, with different ion currents involved in the generation of the complex electrical activity triggered by glucose uptake, although the GSIS process is similar overall [24,26]. These differences do not allow direct translation of the results obtained on mouse to the human case, and stress the importance of characterizing the role of gap junctions in human β-cell dynamics.

In a previous investigation we used patch-clamp recordings obtained in small clusters of β cells, coming from islets of human donors, to estimate gap-junction conductance via a mathematical modeling approach [9]. In particular, we fitted small-amplitude oscillations ($\simeq$10 mV) in membrane potential of patched cells by modeling two mutually coupled cells (doublets), estimating a plausible range of coupling strength ($g_c = 0.010$–0.020 nS/pF) able to explain experimental observations. However, the unknown size of experimental clusters forced us to revise such estimate in this work, by testing larger cellular pools.

Results obtained in three-cell configurations (triplets) and small clusters highlighted the fundamental aspects of the emergent dynamics. Because of biological heterogeneity, several scenarios could in principle generate the experimental membrane potential oscillations, therefore we took into account combinations of coupled silent and spiking cells characterized by different intrinsic frequencies. Overall, our results show that a coupling conductance between 0.005 and 0.020 nS/pF can reproduce experimental small-amplitude oscillations in different cell arrangements, although some configurations are unable to generate signals comparable to the experimental recordings. A very interesting result is the generation of irregular and chaoslike oscillations recovered at selected strengths of the coupling. We previously justified the presence of occasional spikes in the experimental signal as being due to noise fluctuations triggering isolated action potentials. However, considering cell aggregates bigger than cell doublets, we showed here that such behavior can result from chaoslike dynamics where small-amplitude perturbations are occasionally replaced by large oscillations [Fig. 4(f)]. It is not clear how such patterns occur, and a deeper understanding may need nontrivial mathematical analysis of the model of coupled β cells. Such irregular dynamics was found in triplets composed by fast and slow spiking β cells coupled with a silent cell by a gap-junction conductance close to the upper bound of the previously estimated range of g_c, and can be observed also in larger clusters of cells at low coupling strengths [0.005 nS/pF; Fig. 5(f)]. Note that also lower values of coupling supported irregular oscillations in triplets, but without large-amplitude excursions of the membrane potential. Another important finding is that TTX in our simulations was shown to have a regularizing effect on irregular behavior, generating in some cases a frequency reduction of the emergent oscillations. This observation is in line with the changes measured experimentally in the patched cell's membrane potential during TTX exposure (Fig. 1 here; Fig. 2 in Ref. [9]).

Restricting our attention to results obtained on cubic clusters, it is plausible that the upper bound of our estimate is too large to reproduce correctly emergent oscillations, although it is a suitable value to recover experimental signals features in triplets. In this regard, it is plausible that compact clusters overestimate β-cell connectivity in humans where β cells are more scattered through the islet, thus amplifying the

junctional inputs in the model compared to reality. In addition, as noted in mouse [12], it is also possible that adjacent β cells are not electrically coupled. These aspects suggest that percolated rather than compact cellular architectures could be more suited to investigate human β-cell clusters dynamics [30], although the choice of considering a reduced cluster size (27 cells instead of hundreds of cells) and compact arrangements is an acceptable approximation in preliminary studies. Nonetheless, hyperpolarizing gap-junctional currents induced by adjacent silent cells can in principle balance depolarizing currents coming from neighboring active cells, and some cells within the cluster can also show oscillations comparable to experiments for g_c in the range 0.010–0.020 nS/pF depending on the local neighborhood.

For all these reasons our previously estimated range of gap-junction conductance is confirmed by the performed analyses, and slightly corrected to also include lower values. In our new perspective, 0.010 nS/pF has to be taken as physiological mean value more than a lower bound for β-cells coupling, and values down to about 0.005 nS/pF must be considered too. Such revisitation is still consistent with measures performed on rodents and with the heterogeneity in coupling conductances highlighted in mouse islets [12–14]. In light of the importance of electrical coupling suggested by our simulations, we encourage direct electrophysiological studies of the gap-junction strength between β cells in human islets.

Our analyses did not include intrinsic biological noise due to stochastic channel opening, which is known to have a significant role in shaping emergent activity of β-cell aggregates [49–54]. Noise could in principle perturb the observed deterministic dynamics, changing the emergent oscillations' features. However, simulations performed on triplets and clusters with the addition of a white-noise process in the membrane voltage dynamics did not significantly alter the system behavior, suggesting that the observed regimes are robust and may not be destroyed by stochastic fluctuations in ion conductances (see Appendix B). Moreover, we focused our estimation on the fast spiking activity experimentally recorded in humans and we did not consider glycolysis-driven bursting and slow activity (with a characteristic time on the order of minutes) that also occur in human β cells [11]. Our (unpublished) investigations have shown that such slow modulation of fast activity may be included in the model with no changes in the estimation of coupling strength. Specifically, similar perturbations in the silent patched cell can be obtained in the active phases of the slow bursting, both considering homogeneous and heterogeneous glycolytic oscillation frequencies.

Concerning implications of the gap junction conductance estimate in pathological cases, we focused on the emergent behavior of coupled β cells when cells express mutant types of ATP-sensitive potassium channels. These mutant channels are implicated in metabolic disorders leading to hyperglycemia or neonatal diabetes due to an increased excitability or a nonresponsiveness of cells to glucose stimulations, respectively [15–18,21]. Our intent was to analyze the emergent electrical activity in mixed clusters of normal and mutant cells resembling mosaic arrangements realized in engineered mouse islets [37], with the aim to highlight the role of coupling in similar human pathological scenarios. Interestingly, in the case of hyperactive cells, i.e., loss-of-function mutations of KATP, our results show that normally responding cells are unable to keep the KATP-mutated cells silent with $g_c = 0.01$ nS/pF, both at low and high fractions of mutated cells [Figs. 6(c) and 6(d)]. Such findings seem to be in contrast to what was observed in mouse where 30% of normal cells were able to dictate the behavior of the entire population by silencing cells responding prematurely to glucose [37]. In this perspective, a lowering in the coupling conductance by a factor $\geqslant 2$ may at least recover normal response of nonmutant cells, which are otherwise trapped in an active state before the physiological threshold is reached. Regarding gain-of-function mutations, pathological, silent cells evoke a right shift of the dose-response curve due to silencing of the normally activated cells. Such a right shift becomes more pronounced by increasing the fraction of mutant cells. Interestingly, decreasing the junctional conductance by a factor $\simeq 20$ allows the recovery of nonmutant cells from the silencing effect induced by pathological units, thus left shifting the dose-response curve compared to the normally coupled cluster. This behavior is consistent with observations in mouse where a decrease of junctional conductance was shown to restore responsiveness of the islet to glucose [19–21]. The results suggest that, in the case of mutant KATP channels, gap-junction coupling can be a potential therapeutical target to partially restore β-cell function. Moreover, in humans such therapies may be more effective in the case of gain-of-function mutations.

Finally, the study presents limitations that deserve to be outlined. First, the unknown number of cells contained in the experimental clusters still leaves a significant variability in the estimate of the physiological mean value of coupling conductance. Second, the hypothesis that gap-junction currents are responsible for the membrane potential perturbations recorded experimentally still has to be verified, despite being in line with the heterogeneous response of β cells to glucose stimulation. Third, we showed that some properties of the signal, most of all the frequency change of recorded oscillations during TTX exposure, can be reproduced by considering small heterogeneous cells aggregates. Indeed, other aspects could be responsible for these changes, such as a slow ion current overcome by sodium currents in control condition, but driving slow oscillations during TTX exposure. In this regard, it was shown that human β cells express the KCNJ2 gene coding for inwardly rectifying potassium channels (Kir2.1) [55], which are known to affect cardiac activity dynamics [56]. Inclusion of this current into the model supports low-frequency spiking ($\simeq$1–3 Hz) in β cells [57], and it will be taken into account in future investigations. Finally, we focused our study of pathological clusters to the case of mosaic arrangement of normal and mutant cells at fixed percentages. This approach can be used to compare results against experimental observations on engineered mouse islets expressing mosaicism; however, the mosaic pattern may be nonrepresentative of the situation *in vivo*. Further analyses will be devoted to the investigation of pathological cases by considering other arrangements and simultaneous mixing of different mutant types, both loss-of-function and gain-of-function.

Despite the mentioned limitations, the consistency of the outcomes with reported measures on rodents make us confident in our approach. Such findings should be validated in the future

with dedicated experimental procedures as was performed on mouse, and the *in silico* modeling should be extended to percolated architectures other than compact clusters, with the final goal to define the role of coupling in human β-cells dynamics and formulate alternative therapeutical protocols to be adopted in pathological conditions.

ACKNOWLEDGMENTS

A.L. and S.F. were supported by the International Center for Relativistic Astrophysics Network (ICRANet) and Gruppo Nazionale per la Fisica Matematica (GNFM-INdAM). M.G.P. was supported by the University of Padova (PRAt 2012, Progetto Strategico 2011 "DYCENDI"), the European Union's Seventh Framework Programme (FP7-ICT-2011- 9) under Grant Agreement No. 600914 (the MOSAIC consortium) and the European Foundation for the Study of Diabetes (EFSD/Boehringer grant). M.B. was supported by the CIHR (MOP-106435).

A.L. contributed to study design, performed modeling and numerical simulations, analyzed data, and wrote the final manuscript. M.G.P. conceived the general idea of the work, designed research, contributed to modeling, interpreted results, contributed to drafting the manuscript, and revised the final manuscript. M.B. designed and performed all experiments and contributed to the general idea of the work. S.F. contributed to study design and modeling, interpreted results, contributed to drafting the manuscript, and corrected the final manuscript.

APPENDIX A: ELECTROPHYSIOLOGICAL MODEL OF HUMAN β CELL

In the following a complete description of all model equations is given.

The total ion current in Eq. (1) of the paper takes into account all the main currents experimentally recorded from human β cell:

$$
\begin{aligned}
I_{\mathrm{ion},i} &= -(I_{\mathrm{SK}} + I_{\mathrm{BK}} + I_{\mathrm{K}v} + I_{\mathrm{HERG}} + I_{\mathrm{Na}} \\
&\quad + I_{\mathrm{CaL}} + I_{\mathrm{CaPQ}} + I_{\mathrm{CaT}} + I_{\mathrm{KATP}} + I_{\mathrm{leak}}), \\
I_{\mathrm{SK}} &= g_{\mathrm{SK}} \frac{(X_{\mathrm{Ca}_m})^n}{K_{\mathrm{SK}}^n + (X_{\mathrm{Ca}_m})^n}(V - V_{\mathrm{K}}) \\
I_{\mathrm{BK}} &= \bar{g}_{\mathrm{BK}} m_{\mathrm{BK}}[-I_{\mathrm{Ca}}(V) + B_{\mathrm{BK}}](V - V_{\mathrm{K}}), \\
I_{\mathrm{K}v} &= g_{\mathrm{K}v} m_{\mathrm{K}v}(V - V_{\mathrm{K}}), \\
I_{\mathrm{HERG}} &= g_{\mathrm{HERG}} m_{\mathrm{HERG}} h_{\mathrm{HERG}}(V - V_{\mathrm{K}}), \\
I_{\mathrm{Na}} &= g_{\mathrm{Na}} m_{\mathrm{Na},\infty}(V) h_{\mathrm{Na}}(V - V_{\mathrm{Na}}), \\
I_{\mathrm{CaL}} &= g_{\mathrm{CaL}} m_{\mathrm{CaL},\infty}(V) h_{\mathrm{CaL}}(V - V_{\mathrm{Ca}}), \\
I_{\mathrm{CaPQ}} &= g_{\mathrm{CaPQ}} m_{\mathrm{CaPQ},\infty}(V)(V - V_{\mathrm{Ca}}), \\
I_{\mathrm{CaT}} &= g_{\mathrm{CaT}} m_{\mathrm{CaT},\infty}(V) h_{\mathrm{CaT}}(V - V_{\mathrm{Ca}}), \\
I_{\mathrm{KATP}} &= g_{\mathrm{KATP}}(V - V_{\mathrm{K}}), \\
I_{\mathrm{leak}} &= g_{\mathrm{leak}}(V - V_{\mathrm{leak}}).
\end{aligned}
$$

Dynamics of gating variables, modulating the effective conductance for each ion species, is defined through a first-order

TABLE II. Model parameters, as reported in Ref. [9]. Default values used in the paper unless mentioned otherwise.

Parameter	Value	Units
C_m	10	pF
V_{K}	−75	mV
V_{Ca}	65	mV
V_{Na}	70	mV
g_{SK}	0.1	nS/pF
n	5.2	
K_{SK}	0.57	μM
$\bar{g}_{\mathrm{BK}}$	0.02	nS/pA
$V_{m\mathrm{BK}}$	0	mV
$n_{m\mathrm{BK}}$	−10	mV
$\tau_{m\mathrm{BK}}$	2	ms
B_{BK}	20	pA/pF
$g_{\mathrm{K}v}$	1	nS/pF
$V_{m\mathrm{K}v}$	0	mV
$n_{m\mathrm{K}v}$	−10	mV
$\tau_{m\mathrm{K}v,0}$	2	ms
g_{HERG}	0	nS/pF
$V_{m\mathrm{HERG}}$	−30	mV
$V_{h\mathrm{HERG}}$	−42	mV
$n_{m\mathrm{HERG}}$	−10	mV
$n_{h\mathrm{HERG}}$	17.5	mV
$\tau_{m\mathrm{HERG}}$	100	ms
$\tau_{h\mathrm{HERG}}$	50	ms
g_{Na}	0.4	nS/pF
$V_{m\mathrm{Na}}$	−18	mV
$V_{h\mathrm{Na}}$	−42	mV
$n_{m\mathrm{Na}}$	−5	mV
$n_{h\mathrm{Na}}$	6	mV
$\tau_{h\mathrm{Na}}$	2	ms
g_{CaL}	0.14	nS/pF
$V_{m\mathrm{CaL}}$	−25	mV
$n_{m\mathrm{CaL}}$	−6	mV
$\tau_{h\mathrm{CaL}}$	20	ms
g_{CaPQ}	0.17	nS/pF
$V_{m\mathrm{CaPQ}}$	−10	mV
$n_{m\mathrm{CaPQ}}$	−6	mV
g_{CaT}	0.05	nS/pF
$V_{m\mathrm{CaT}}$	−40	mV
$V_{h\mathrm{CaT}}$	−64	mV
$n_{m\mathrm{CaT}}$	−4	mV
$n_{h\mathrm{CaT}}$	8	mV
$\tau_{h\mathrm{CaT}}$	7	ms
g_{KATP}	0.01	nS/pF
g_{leak}	0.015	nS/pF
V_{leak}	−30	mV
K_{SERCA}	0.27	μM
K_{PMCA}	0.50	μM
$J_{\mathrm{SERCA}}^{\mathrm{max}}$	0.06	μM/ms
$J_{\mathrm{PMCA}}^{\mathrm{max}}$	0.021	μM/ms
$J_{\mathrm{NCX},0}$	0.01867	ms^{-1}
J_{leak}	0.00094	μM/ms
f	0.01	
B	0.1	ms^{-1}
Vol_c	1.15×10^{-12}	L
Vol_m	0.1×10^{-12}	L
α	5.18×10^{-15}	μmol/pA/ms

differential equation of the form

$$\frac{dm_X}{dt} = \frac{m_{X,\infty}(V) - m_X}{\tau_{mX}},$$

where τ_{mX} (τ_{hX}) represents the activation (inactivation) time constant, and $m_{X,\infty}(V)$ ($h_{X,\infty}(V)$) is the steady-state activation (inactivation) of ion channels, which depends on the membrane voltage.

Activation (inactivation) functions are described through the classic Boltzmann formulation:

$$m_{X,\infty}(V) = \frac{1}{1 + \exp\left[(V - V_{mX})/n_{mX}\right]};$$

except for the inactivation of L-type calcium channels, which depends on their activation level:

$$S = \min\{1, 1 + [m_{\mathrm{CaL},\infty}(V)(V - V_{\mathrm{Ca}})]/57\ \mathrm{mV}\},$$
$$h_{\mathrm{CaL},\infty}(V) = \max\{0, S\}.$$

Voltage dependence of (delayed-rectifying) potassium channels time constant is modeled as

$$\tau_{m\mathrm{K}v} = \begin{cases} \tau_{m\mathrm{K}v,0} + 10 \exp\left(\frac{-20\ \mathrm{mV} - V}{6\ \mathrm{mV}}\right)\ \mathrm{ms}, & \text{for } V \geqslant 26.6\ \mathrm{mV}, \\ \tau_{m\mathrm{K}v,0} + 30\ \mathrm{ms}, & \text{for } V < 26.6\ \mathrm{mV}. \end{cases}$$

In addition, the intracellular calcium concentration is computed with a two-compartment model, taking into account ions accumulation within a thin layer ($\simeq$190 nm) under the cell membrane and calcium diffusion in the cytoplasm bulk. Voltage-gated currents, membrane exchangers, SERCA pumps, and leakage factors are included in the dynamics:

$$\begin{aligned} \frac{dX_{\mathrm{Ca}_m}}{dt} &= f\alpha C_m(-I_{\mathrm{CaL}} - I_{\mathrm{CaPQ}} - I_{\mathrm{CaT}})/\mathrm{Vol}_m \\ &\quad - f(\mathrm{Vol}_c/\mathrm{Vol}_m)[B(X_{\mathrm{Ca}_m} - X_{\mathrm{Ca}_c}) \\ &\quad + (J_{\mathrm{PMCA}} + J_{\mathrm{NCX}})], \\ \frac{dX_{\mathrm{Ca}_c}}{dt} &= f[B(X_{\mathrm{Ca}_m} - X_{\mathrm{Ca}_c}) - J_{\mathrm{SERCA}} + J_{\mathrm{leak}}], \end{aligned}$$

where X_{Ca_m} and X_{Ca_c} are the submembrane and bulk intracellular calcium concentrations, respectively. Calcium fluxes due to SERCA pumps and other exchangers are

$$J_{\mathrm{SERCA}} = J^{\max}_{\mathrm{SERCA}} \frac{(X_{\mathrm{Ca}_c})^2}{K^2_{\mathrm{SERCA}} + (X_{\mathrm{Ca}_c})^2},$$
$$J_{\mathrm{PMCA}} = J^{\max}_{\mathrm{PMCA}} \frac{X_{\mathrm{Ca}_m}}{K_{\mathrm{PMCA}} + X_{\mathrm{Ca}_m}},$$
$$J_{\mathrm{NCX}} = J_{\mathrm{NCX},0}\, X_{\mathrm{Ca}_m}.$$

All parameter values are given in Table II.

APPENDIX B: COMMENT ON NOISE EFFECT

Intrinsic biological noise due to stochastic channel gating is an important feature of β-cell dynamics. Several modeling studies have shown that noise significantly affects the emergent bursting period of coupled mouse β cells [49–54], and contributes to synchronization of cells both in compact and sparse architectures [27,28,30]. However, the relative importance of noise compared to cell-to-cell variability (heterogeneity) is still debated in the literature, and similar experimental observations reproduced by stochastic formulations of β-cell dynamics are also explained by heterogenous deterministic models [58–61]. Indeed, it has been suggested that the effects of stochastic events are due to heterogeneity masquerading as noise [52].

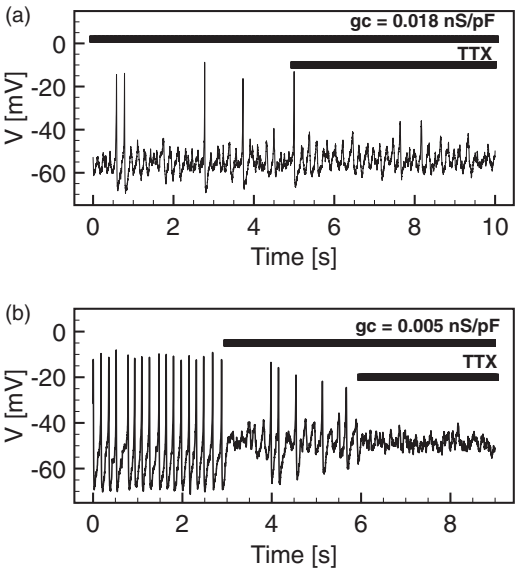

FIG. 7. Simulations of a triplet and small cluster computed with independent and additive Gaussian white-noise processes on the membrane voltage dynamics of each cell. (a) HF-S-LF chain as in Fig. 4(f). (b) 27-cells cluster as in Fig. 5(f). Strength of noise σ was set to 0.5.

In this study we preferred to use a deterministic formulation of β-cell electrophysiology because of the strong heterogeneity in cell parameters. Such a choice allowed us to analyze the underlying dynamics with classical theory of complex dynamical systems. However, since stochastic effects may significantly perturb the deterministic solutions, we further checked the impact of noise on membrane potential dynamics.

In line with Ref. [10], we modified Eq. (1) in the paper by adding a stochastic input $\sigma\Gamma_t$, where σ is a modulating factor, and Γ_t represents a Gaussian white-noise process with zero mean and covariance $\langle\Gamma(t)\,\Gamma(t')\rangle = \delta(t - t')$. We modeled triplets and clusters as in Figs. 4(f) and 5(f), by adding independent noise processes to each cells' voltage dynamics. Results are shown in Fig. 7. Noise affects emergent oscillations both in the triplet and the cluster; an increased number of action potentials in control conditions and more irregular oscillations during TTX exposure can be observed. However, the underlying dynamics is qualitatively conserved: small-amplitude oscillations coexist with occasional action potentials which are suppressed by sodium channels block. This analysis suggests that the quantitative features of the deterministic dynamics modeled in the paper are robust to stochastic perturbations, and that our conclusions still hold when considering cellular noise in addition to cell heterogeneity.

[1] R. M. Santos, L. M. Rosario, A. Nadal, J. Garcia-Sancho, B. Soria, and M. Valdeolmillos, Pflügers Arch. **418**, 417 (1991).

[2] P. Bergsten, E. Grapengiesser, E. Gylfe, A. Tengholm, and B. Hellman, J. Biol. Chem. **269**, 8749 (1994).

[3] F. C. Jonkers, J.-C. Jonas, P. Gilon, and J.-C. Henquin, J. Physiol. **520**, 839 (1999).

[4] J. V. Rocheleau, G. M. Walker, W. S. Head, O. P. McGuinness, and D. W. Piston, Proc. Natl. Acad. Sci. USA **101**, 12899 (2004).

[5] M. A. Ravier, M. Güldenagel, A. Charollais, A. Gjinovci, D. Caille, G. Söhl, C. B. Wollheim, K. Willecke, J.-C. Henquin, and P. Meda, Diabetes **54**, 1798 (2005).

[6] S. Speier, A. Gjinovci, A. Charollais, P. Meda, and M. Rupnik, Diabetes **56**, 1078 (2007).

[7] W. S. Head, M. L. Orseth, C. S. Nunemaker, L. S. Satin, D. W. Piston, and R. K. Benninger, Diabetes **61**, 1700 (2012).

[8] V. Serre-Beinier, D. Bosco, L. Zulianello, A. Charollais, D. Caille, E. Charpantier, B. R. Gauthier, G. R. Diaferia, B. N. Giepmans, R. Lupi *et al.*, Hum. Mol. Genet. **18**, 428 (2009).

[9] A. Loppini, M. Braun, S. Filippi, and M. G. Pedersen, Phys. Biol. **12**, 066002 (2015).

[10] M. G. Pedersen, Biophys. J. **99**, 3200 (2010).

[11] M. Riz, M. Braun, and M. G. Pedersen, PLoS J. Comput. Biol. **10**, e1003389 (2014).

[12] M. Pérez-Armendariz, C. Roy, D. C. Spray, and M. Bennett, Biophys. J. **59**, 76 (1991).

[13] E. Andreu, B. Soria, and J. V. Sanchez-Andres, J. Physiol. **498**, 753 (1997).

[14] Q. Zhang, J. Galvanovskis, F. Abdulkader, C. J. Partridge, S. O. Göpel, L. Eliasson, and P. Rorsman, Philos. Trans. R. Soc. A **366**, 3503 (2008).

[15] E. A. Cartier, L. R. Conti, C. A. Vandenberg, and S.-L. Shyng, Proc. Natl. Acad. Sci. USA **98**, 2882 (2001).

[16] J. Koster, M. Remedi, T. Flagg, J. Johnson, K. Markova, B. Marshall, and C. Nichols, Proc. Natl. Acad. Sci. USA **99**, 16992 (2002).

[17] S. Ellard, S. E. Flanagan, C. A. Girard, A.-M. Patch, L. W. Harries, A. Parrish, E. L. Edghill, D. J. Mackay, P. Proks, K. Shimomura *et al.*, Am. J. Hum. Genet. **81**, 375 (2007).

[18] Y. Quan, A. Barszczyk, Z.-p. Feng, and H.-s. Sun, Acta Pharmacol. Sin. **32**, 765 (2011).

[19] R. K. Benninger, M. Remedi, W. Head, A. Ustione, D. Piston, and C. Nichols, Diabetologia **54**, 1087 (2011).

[20] L. M. Nguyen, M. Pozzoli, T. H. Hraha, and R. K. Benninger, Diabetes **63**, 1685 (2014).

[21] A. M. Notary, M. J. Westacott, T. H. Hraha, M. Pozzoli, and R. K. Benninger, PLoS Comput. Biol. **12**, e1005116 (2016).

[22] S. Misler, D. W. Barnett, K. D. Gillis, and D. M. Pressel, Diabetes **41**, 1221 (1992).

[23] D. W. Barnett, D. M. Pressel, and S. Misler, Pflügers Arch. **431**, 272 (1995).

[24] M. Braun, R. Ramracheya, M. Bengtsson, Q. Zhang, J. Karanauskaite, C. Partridge, P. R. Johnson, and P. Rorsman, Diabetes **57**, 1618 (2008).

[25] D. A. Jacobson, F. Mendez, M. Thompson, J. Torres, O. Cochet, and L. H. Philipson, J. Physiol. **588**, 3525 (2010).

[26] P. Rorsman and M. Braun, Annu. Rev. Physiol. **75**, 155 (2013).

[27] A. Sherman and J. Rinzel, Biophys. J. **59**, 547 (1991).

[28] A. Loppini, A. Capolupo, C. Cherubini, A. Gizzi, M. Bertolaso, S. Filippi, and G. Vitiello, Phys. Lett. A **378**, 3210 (2014).

[29] T. H. Hraha, M. J. Westacott, M. Pozzoli, A. M. Notary, P. M. McClatchey, and R. K. P. Benninger, PLoS Comput. Biol. **10**, e1003819 (2014).

[30] C. Cherubini, S. Filippi, A. Gizzi, and A. Loppini, Phys. Rev. E **92**, 042702 (2015).

[31] M. Brissova, M. J. Fowler, W. E. Nicholson, A. Chu, B. Hirshberg, D. M. Harlan, and A. C. Powers, J. Histochem. Cytochem. **53**, 1087 (2005).

[32] O. Cabrera, D. M. Berman, N. S. Kenyon, C. Ricordi, P.-O. Berggren, and A. Caicedo, Proc. Natl. Acad. Sci. USA **103**, 2334 (2006).

[33] D. J. Steiner, A. Kim, K. Miller, and M. Hara, Islets **2**, 135 (2010).

[34] A. Nittala, S. Ghosh, and X. Wang, PLoS ONE **2**, e983 (2007).

[35] G. Cappon and M. G. Pedersen, Chaos **26**, 053103 (2016).

[36] B. Ermentrout, *Simulating, Analyzing, and Animating Dynamical Systems: A Guide To Xppaut for Researchers and Students* (Society for Industrial and Applied Mathematics, Philadelphia, 2002).

[37] J. V. Rocheleau, M. S. Remedi, B. Granada, W. S. Head, J. C. Koster, C. G. Nichols, and D. W. Piston, PLoS Biol. **4**, e26 (2006).

[38] D. Salomon and P. Meda, Exp. Cell Res. **162**, 507 (1986).

[39] D. Bosco, L. Orci, and P. Meda, Exp. Cell Res. **184**, 72 (1989).

[40] P. Meda, D. Bosco, M. Chanson, E. Giordano, L. Vallar, C. Wollheim, and L. Orci, J. Clin. Invest. **86**, 759 (1990).

[41] F. C. Jonkers and J.-C. Henquin, Diabetes **50**, 540 (2001).

[42] F. Allagnat, P. Klee, M. Peyrou, D. Martin, A. Charollais, D. Caille, J.-A. Haefliger, and P. Meda, in *Diabetologia* (Springer, New York, 2007), Vol. 50, p. S45.

[43] F. Allagnat, F. Alonso, D. Martin, A. Abderrahmani, G. Waeber, and J.-A. Haefliger, J. Biol. Chem. **283**, 5226 (2008).

[44] P. Klee, F. Allagnat, H. Pontes, M. Cederroth, A. Charollais, D. Caille, A. Britan, J.-A. Haefliger, and P. Meda, J. Clin. Invest. **121**, 4870 (2011).

[45] F. Allagnat, P. Klee, A. K. Cardozo, P. Meda, and J. Haefliger, Cell Death Differ. **20**, 1742 (2013).

[46] N. L. Farnsworth, R. L. Walter, A. Hemmati, M. J. Westacott, and R. K. Benninger, J. Biol. Chem. **291**, 3184 (2016).

[47] R. L. Michaels and J. D. Sheridan, Science **214**, 801 (1981).

[48] P. Meda, R. Santos, and I. Atwater, Diabetes **35**, 232 (1986).

[49] A. Sherman, J. Rinzel, and J. Keizer, Biophys. J. **54**, 411 (1988).

[50] G. De Vries and A. Sherman, J. Theor. Biol. **207**, 513 (2000).

[51] J. Jo, H. Kang, M. Y. Choi, and D.-S. Koh, Biophys. J. **89**, 1534 (2005).

[52] M. G. Pedersen, J. Theor. Biol. **235**, 1 (2005).

[53] M. G. Pedersen and M. P. Sørensen, SIAM J Appl. Math. **67**, 530 (2007).

[54] M. G. Pedersen, J. Theor. Biol. **248**, 391 (2007).

[55] B. Kutlu, D. Burdick, D. Baxter, J. Rasschaert, D. Flamez, D. L. Eizirik, N. Welsh, N. Goodman, and L. Hood, BMC Med. Genomics **2**, 1 (2009).

[56] P. L. Hedley, P. Jørgensen, S. Schlamowitz, R. Wangari, J. Moolman-Smook, P. A. Brink, J. K. Kanters, V. A. Corfield, and M. Christiansen, Hum. Mutat. **30**, 1486 (2009).

[57] M. Riz, M. Braun, X. Wu, and M. G. Pedersen, Biochem. Biophys. Res. Commun. **459**, 284 (2015).
[58] P. Smolen, J. Rinzel, and A. Sherman, Biophys. J. **64**, 1668 (1993).
[59] A. Sherman, Am. J. Physiol. **271**, E362 (1996).
[60] G. De Vries, A. Sherman, and H.-R. Zhu, Bull. Math. Biol. **60**, 1167 (1998).
[61] M. G. Pedersen, J. Diabetes Sci. Technol. **3**, 12 (2009).